AGU PUBLICATIONS

JGR

Journal of Geophysical Research: Space Physics

RESEARCH ARTICLE
10.1002/2015JA021183

Special Section:
Variability of the Sun and Its Terrestrial Impact VarSITI

The 27 day solar rotational effect on mesospheric nighttime OH and O_3 observations induced by geomagnetic activity

T. Fytterer[1], M. L. Santee[2], M. Sinnhuber[1], and S. Wang[2]

[1]Institute for Meteorology and Climate Research, Karlsruhe Institute of Technology, Eggenstein-Leopoldshafen, Germany, [2]Jet Propulsion Laboratory, California Institute of Technology, Pasadena, California, USA

Key Points:
- Analysis of mesospheric nighttime OH and O_3 satellite observations at auroral latitudes
- The 27 day solar rotational signal in nighttime OH and O_3 induced by geomagnetic activity
- Nonlinear relation between OH and O_3 at 75 km in the Northern and Southern Hemisphere

Supporting Information:
- Figures S1 and S2

Correspondence to:
T. Fytterer,
tilo.fytterer@kit.edu

Citation:
Fytterer, T., M. L. Santee, M. Sinnhuber, and S. Wang (2015), The 27 day solar rotational effect on mesospheric nighttime OH and O_3 observations induced by geomagnetic activity, *J. Geophys. Res. Space Physics*, *120*, 7926–7936, doi:10.1002/2015JA021183.

Received 3 MAR 2015
Accepted 6 AUG 2015
Accepted article online 13 AUG 2015
Published online 10 SEP 2015

Abstract Observations performed by the Earth Observing System Microwave Limb Sounder instrument on board the Aura satellite from 2004 to 2009 (2004 to 2014) were used to investigate the 27 day solar rotational cycle in mesospheric OH (O_3) and the physical connection to geomagnetic activity. Data analysis was focused on nighttime measurements at geomagnetic latitudes connected to the outer radiation belts (55°N/S–75°N/S). The applied superposed epoch analysis reveals a distinct 27 day solar rotational signal in OH and O_3 during winter in both hemispheres at altitudes >70 km. The OH response is positive and in-phase with the respective geomagnetic activity signal, lasting for 1–2 days. In contrast, the O_3 feedback is negative, delayed by 1 day, and is present up to 4 days afterward. Largest OH (O_3) peaks are found at ~75 km, exceeding the 95% significance level and the measurement noise of <2% (<0.5%), while reaching variations of +14% (−7%) with respect to their corresponding background. OH at 75 km is observed to respond to particle precipitation only after a certain threshold of geomagnetic activity is exceeded, depending on the respective OH background. The relation between OH and O_3 at 75 km in both hemispheres is found to be nonlinear. In particular, OH has a strong impact on O_3 for relatively weak geomagnetic disturbances and accompanying small absolute OH variations (<0.04 ppb). In contrast, catalytic O_3 depletion is seen to slow down for stronger geomagnetic variations and OH anomalies (0.04–0.13 ppb), revealing small variations around −0.11 ppm.

1. Introduction

Electrons with energy levels of several keV–MeV can enter mesospheric regions while guided by the Earth's magnetic field lines, primarily between 55° and 75° geomagnetic latitudes, which are equivalent to the area of the aurora region/radiation belts. This particle precipitation leads to the production of odd hydrogen ($HO_x = H + OH + HO_2$) from water vapor via positive ion chemistry involving water clusters [e.g., *Solomon et al.*, 1981]. However, this process is only efficient at altitudes from 60 to 80 km. Furthermore, HO_x is responsible for the catalytic O_3 depletion at these mesospheric heights [e.g., *Lary*, 1997], but the direct impact is restricted to the source region due to the short chemical lifetime of HO_x of less than 1 day at altitudes <80 km [*Brasseur and Solomon*, 2005, Figure 5.27]. Considering that O_3 is a major contributor to radiatively induced heating and cooling rates at mesospheric altitudes below ~80 km, further impact on temperature and circulation is possible.

Satellite observations presented by *Damiani et al.* [2008] showed that at high latitudes (75°–82°) during winter 2005, solar particle events lead to the formation of OH, which is accompanied by O_3 depletion. More recently, *Andersson et al.* [2012] analyzed OH satellite data from 2004 to 2009. They found a measurable positive effect from electron precipitation on OH from 70 to 78 km at 55°–65° geomagnetic latitudes. The pattern is similar in both hemispheres but more obvious in the Northern Hemisphere. The continuation study by *Andersson et al.* [2014] also revealed considerable O_3 depletion at similar altitudes observed in three different satellite data sets from 2002 to 2012. The 27 day solar rotational cycle in tropical mesospheric OH satellite data was reported by *Shapiro et al.* [2012], while *Ruzmaikin et al.* [2007] observed the solar 27 day effect in stratospheric O_3 at high latitudes during winter. However, the latter two studies focused on daytime photochemical responses to solar irradiance variability during the 27 day cycle. In contrast, the relation between the 27 day solar rotational cycle in geomagnetic activity and OH/O_3 measurements has, to our knowledge, not been investigated. *Friederich et al.* [2014], however, showed that the 27 day signal in both solar UV radiation and geomagnetic activity influences NO_2 near the stratopause region.

Table 1. Summary of Used Trace Gas Altitudes[a]

Pressure Level (Pa)	Approximated Height (km)	OH Availability	O_3 Availability
21.44	60	yes	yes
14.68	63	yes	yes
10	65	yes	yes
6.81	68	yes	---
4.64	70	yes	yes
3.16	73	yes	---
2.15	75	yes	yes
1.47	78	yes	---
1	81	yes	---

[a]MLS Aura satellite pressure levels, the corresponding altitudes, and availability for OH and O_3 measurements.

In this study we focus on nighttime OH (2004–2009) and O_3 (2004–2014) volume mixing ratios (vmrs) from 60 to 81 km, observed by the Earth Observing System (EOS) Microwave Limb Sounder (MLS) instrument on board the Aura satellite. We individually analyze the relation between the geomagnetic *Ap* index, OH, and O_3 during summer and winter conditions in both hemispheres between geomagnetic latitudes 55° and 75° with respect to the 27 day solar rotational signal.

2. Data and Method

2.1. Data Filtering

The EOS MLS instrument on board the Sun-synchronous near-polar orbit Aura satellite has been nearly continuously operating since August 2004 [*Waters et al*., 2006]. The MLS instrument measures atmospheric species such as OH and O_3 among other trace gases during both day and night, using thermal emission of the rotational lines in the millimeter and submillimeter wavelength range. In this study we use the level 2 OH vmr (proxy for HO_x) and O_3 vmr data version 3.3/3.4 [*Livesey et al*., 2013]. The complete data set of O_3 vmr observations [*Froidevaux et al*., 2008] from August 2004 to August 2014 was analyzed, but a continuous OH vmr time series [*Pickett et al*., 2008] is only available from August 2004 to December 2009 due to aging of the corresponding radiometer.

Assuming that the particle precipitation impact is more important during the absence of H_2O photolysis and the accompanying higher OH background, the focus was set on night measurements (solar zenith angle $>$96°). Nightly mean zonal means, covering 55°N/S–75°N/S geomagnetic latitudes, were calculated, if at least 50 accepted profiles were available. The geomagnetic latitudes were calculated by assuming a symmetrical dipole field and considering a wandering Earth's magnetic field pole. This algorithm was repeated for every retrieved OH (O_3) height level (Table 1), ranging from 60 to 81 km (60 to 75 km). The presented altitudes are estimated from the respective pressure level of MLS observations and are used as the vertical coordinate in this study. Note that the lack of O_3 availability at 68 and 73 km is due to the coarser retrieval grid used for O_3 at pressures less than 0.1 hPa. Additionally, the calculation was individually performed for the Northern Hemisphere (NH) and Southern Hemisphere (SH) as well as for summer and winter conditions, defined by spring and autumn equinox. In detail NH summer/SH winter covers the period from 22 March to 19 September, while SH summer/NH winter extends from 24 September to 19 March.

Furthermore, the impact of large solar proton events (SPEs) was removed. A day was assumed to be considerably influenced by a large SPE if the corresponding $>$10 MeV proton flux, measured by the Geostationary Operational Environmental Satellites, exceeded the empirically determined threshold of 400 protons $cm^{-2}\,s^{-1}\,sr^{-1}$. Note that this threshold is about 40 times larger than then commonly limit used to exclude SPEs, which is considered in the respective discussions. Additionally, the complete period between 1 day before an SPE and 5 (10) days afterward for OH (O_3) was excluded from further investigations. These limits were determined empirically, based on observations of SPE-induced OH and O_3 variations reported by *Damiani et al*. [2008].

The *Ap* index (*Ap*), which is used here as a proxy for planetary geomagnetic disturbances in the ionosphere/magnetosphere, is derived from ground-based magnetometer measurements located at 13 different observatories between 46° and 63° geomagnetic latitudes. Note that the *Ap* provides no information about the actual fluxes or the particle energy levels nor the underlying source mechanisms causing the disturbance. But it is still a suitable indicator to estimate the magnitude of overall turbulence in the ionosphere/magnetosphere, which is equivalent to the occurrence probability of precipitating particles. Variations in the *Ap* arise from a combination of several mechanisms and include periodic and nonperiodic events of different time scales. The 27 day solar rotational signal in *Ap* is a persistent feature and generally evolves from corotating interaction regions (CIRs), which originate from long-lived coronal holes and

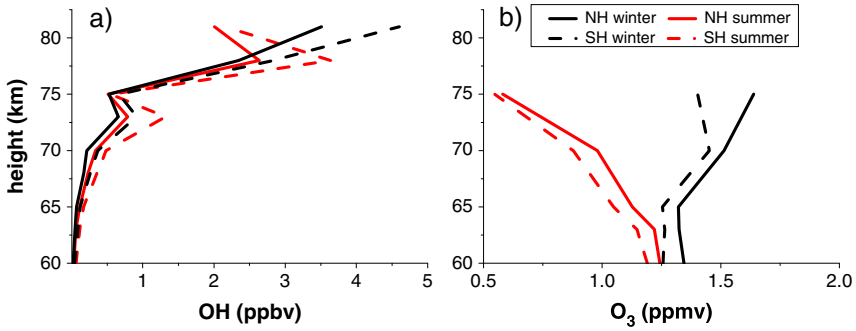

Figure 1. Climatology of (a) OH and (b) O_3 for winter and summer conditions between 55°N/S and 75°N/S geomagnetic latitudes, derived from MLS Aura satellite nighttime observations from 2004 to 2009 (OH) and 2004 to 2014 (O_3).

contribute about 30%/70% to geomagnetic activity during solar maximum/outside the solar maximum [*Richardson et al.*, 2000]. In comparison to coronal mass ejections (CMEs), CIRs are relatively weak and long lasting, while most of the energetic precipitating particles are delayed by a few days with respect to the *Ap* peak.

2.2. Superposed Epoch Analysis

A superposed epoch analysis (SEA) [*Chree*, 1913] was performed to investigate the mesospheric OH and O_3 response to particle precipitation. In the first step, the difference between the trace gas measurement (OH or O_3) of a certain day and the corresponding 27 day running mean centered at the day was calculated, representing the absolute deviation of the respective background (27 day running mean). This absolute difference was divided by the 27 day running mean and eventually multiplied by the factor of 100% for more convenient values. The results are referred to as OH or O_3 amplitude here. We subtracted the 27 day running mean to minimize O_3 variations with frequencies $<1/27\ d^{-1}$. Note that the Sun's rotational cycle is not exactly 27 day, but a sensitivity study revealed that changing the window size between 25 and 30 days leads to negligible differences in SEA results (not shown here). Furthermore, amplitudes were derived instead of absolute differences due to the considerable variability of trace gas vmrs with height, hemisphere, and season, as shown by the 5/10 year OH/O_3 climatology (Figure 1). In detail, OH vmrs are generally low at altitudes below 70 km (<0.5 ppb), but show strong increases above 75 km, which was also observed by *Pickett et al.* [2006]. O_3 is less variable compared to OH and reveals decreasing/increasing values with height during summer/winter. Seasonal variations in OH and O_3 are likely caused by the fact that the zonal mean nighttime measurements used here are closer to the pole during winter (~65°N/S geomagnetic latitudes) but shifted to lower geomagnetic mean latitudes in summer (~60°N/S). Furthermore, OH vmrs are slightly higher in the SH, while the opposite behavior is observed for O_3 vmrs. These interhemispheric differences might result from generally higher SH temperature and SH water vapor background, which could lead to increased OH abundance [*Andersson et al.*, 2012] and eventually reduce the O_3 background compared to that in the NH.

In the next step, a day was defined as an event day if the difference between *Ap* value of this day and the corresponding 27 day running *Ap* mean exceeds 1 standard deviation of the *Ap* value. Additionally, the respective OH or O_3 amplitude has to be actually available at this day. The first criterion leads to the fact that smaller absolute *Ap* variations are regarded as an event during low geomagnetic activity, because the corresponding standard deviation of the *Ap* is small as well. Consequently, these events contribute to a lesser degree to the overall SEA response and all event days are more or less uniformly distributed through the complete time interval. Both selection criteria were chosen to obtain at least 50 event days per hemisphere-season interval to increase the statistical significance. In detail, the applied limits lead to 58 (NH summer), 123 (SH summer), 141 (NH winter), and 122 (SH winter) events for OH measurements. The number of event days for O_3 observations (117 NH summer, 209 SH summer, 245 NH winter, and 228 SH winter) is approximately doubled due to the longer O_3 data set. Lower numbers of event days originate from data gaps (not shown here). Further, note that successive event days are possible, if the respective criteria are valid. Finally, the daily *Ap* averages, as well as the OH and O_3 amplitudes of ±30 days around all events, were

individually arithmetically averaged to calculate the SEA signal. The SEA time interval of ±30 days was chosen to investigate the 27 day solar rotation cycle.

The significance of the obtained trace gas amplitudes and *Ap* signal was tested, using the error of the 27 day running mean while assuming the worst case of an absolute error propagation. The trace gas amplitudes were further validated by using the precision value, representing the radiance noise in the measurements that influences the retrieval of the trace gas data. The precision values of the individual data points were assumed to propagate independently throughout the calculation of the zonal mean and the SEA. As an intermediate step, the calculated zonal mean precision was divided by the respective zonal mean and multiplied by a factor of 100, and this relative precision error was used afterward.

3. Results and Discussion

3.1. The 27 Day Signal in *Ap* Index, OH, and O_3

The results of the SEA for *Ap* during NH and SH winter for both OH and O_3 observation periods are displayed in Figures 2a and 2b, representing the general *Ap* characteristics. The *Ap* signals obtained reveal a distinct 27 day cycle in each hemisphere for both OH and O_3 measurement periods, showing a major peak at day 0 (=event day) and two secondary maxima at the days ±27. Note that no sharp peaks, restricted to only 1 day, are observed because successive days can be considered as event days, and the major fraction of precipitating energetic particles induced by CIR storms might be delayed by a few days with respect to the *Ap* peak. All three peaks are above the significance level of 99%, except for the secondary maxima of the investigated O_3 time interval, which still exceed the significance level of 95%. Also, weakly visible, but well below, the 2σ confidence level in both observation periods and hemispheres is minor maxima close to the days ±9 and ±18, which might be attributed to additionally occurring coronal holes on the Sun that lead to more than one CIR storm within the same period. Since the *Ap* and subsequently the SEA cannot distinguish between the individual sources of the geomagnetic disturbance, the observed 27 day signal in *Ap* is probably a combination of both CMEs and CIRs. This overlapping impact is supported by the generally larger maximum at day zero in comparison to the secondary peaks. Furthermore, the OH observation period overlapped with the declining phase of the solar cycle, and consequently, geomagnetic activity was dominated by CIRs and influenced to a lesser degree by CMEs [*Richardson et al*., 2000]. This might explain the fact that the secondary peaks are stronger during the OH period than in the O_3 time interval, which is true for absolute values as well as with respect to the corresponding major maximum, because a pure CIR-induced 27 day signal would reveal three maxima of similar amplitude.

In order to analyze the relation between *Ap*, OH, and O_3 in more detail, the OH and O_3 amplitudes of both hemispheres during winter conditions at 75 km are displayed in Figures 2c and 2d. This altitude-season interval was chosen because the largest OH (O_3) peaks are found at ~75 km, consistent with the results reported by *Andersson et al*. [2014]. The NH OH amplitude (Figure 2c) closely follows the *Ap* signal (Figure 2a), also revealing a pronounced 27 day cycle marked by a major peak at day 0 and two secondary maxima at day ±27, which are about half as strong as the major one. Note that the three peaks in *Ap* and OH are not suitable to quantify the relationship between *Ap* and OH, since there might be a threshold of geomagnetic activity which has to be exceeded before OH enhancement is initialized (see section 3.3). Furthermore, these three maxima are closely surrounded by negative OH amplitudes, which are caused by the subtraction of the 27 day running mean (see section 2.1). This fact might also partly contribute to missing apparent positive OH amplitudes around day ±9 and day ±18. Additionally, the respective *Ap* signal is below the 95% significance level. Considering that the significance level was estimated by using the error of the 27 day running mean, larger errors are associated with the maxima due to the generally larger variability on these days. Thus, the final error value depends on the SEA day (e.g., see Figure 2a). However, it is more reasonable to evaluate the maximum trace gas amplitudes in comparison to the error of the background. In this case the term "background" refers to the period of weak *Ap* signals in the investigated SEA interval. Based on Figures 2a and 2b, the error of *Ap* quiet time is defined by the arithmetic average of all errors from day −20 to −5 and +5 to +20. Consequently, the significance of the trace gas amplitudes was estimated using the constant error of *Ap* quiet time, revealing that the peaks at day 0 and day −27 exceed the significance level of 95%. In the SH an in-phase OH response associated with *Ap* is also visible at day 0, which is above the 95% significance level. In contrast, the secondary peaks are missing, and the pattern is generally noisier compared to

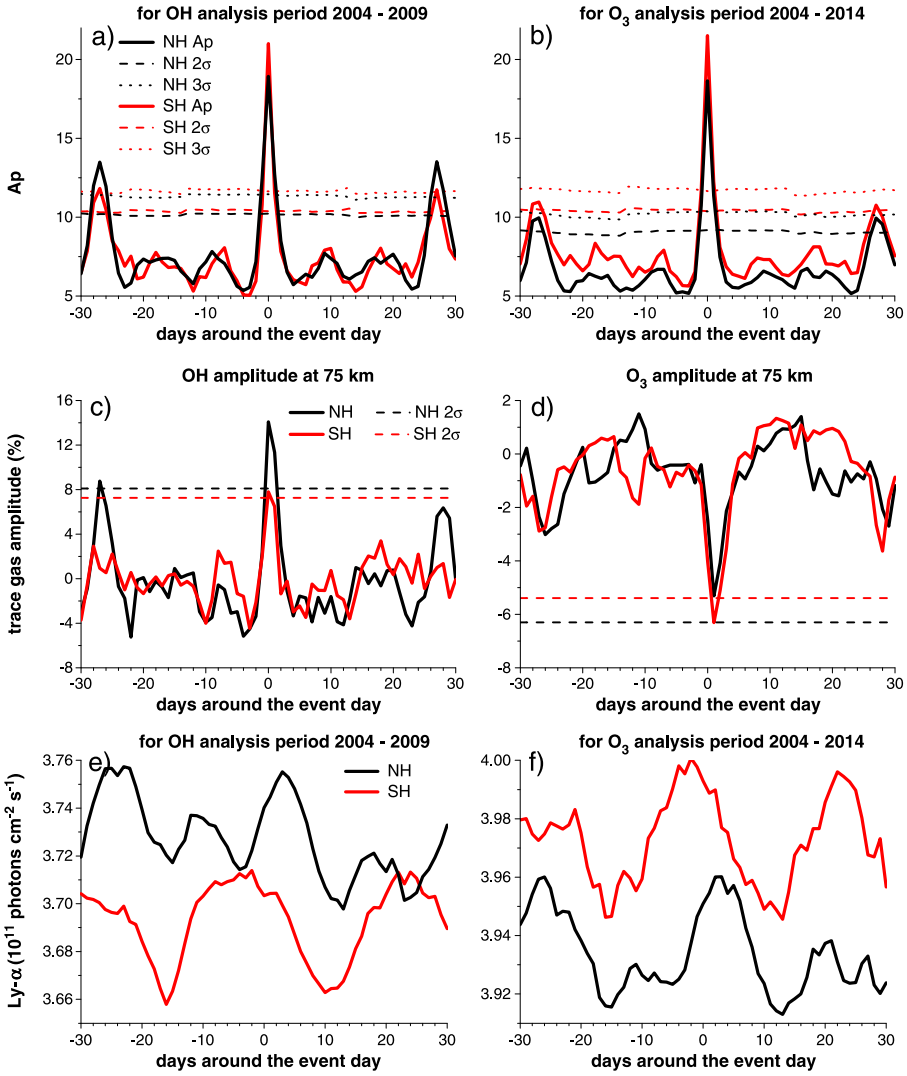

Figure 2. (top row) Superposed epoch analysis for the signal of the *Ap* index for the period of (a) OH and (b) O_3 observations during winter. (middle row) The respective (c) OH and (d) O_3 amplitudes at 75 km during winter conditions between 55°N/S and 75°N/S geomagnetic latitudes, using MLS Aura satellite OH and O_3 nighttime measurements. (bottom row) The corresponding Lyman alpha results. Note the different scaling in all panels.

the NH as discussed in the next section. The linear correlation coefficient between the SEA time series of *Ap* and the respective OH amplitude is about +0.87 in the NH and +0.70 in the SH.

It is therefore reasonable to use *Ap* as a proxy for OH enhancement and compare the *Ap* signal with the O_3 amplitude. The general structure and magnitude of the O_3 amplitude is similar in both hemispheres, revealing a pronounced 27 day cycle, which is delayed by +1 day compared to the signal in *Ap* and OH. The three O_3 amplitude maxima show measurable negative values for several days after the largest response, but only the major maximum at day +1 in the SH exceeds the 95% significance level. However, the overall relation between *Ap* signal and O_3 amplitude is still strong, showing linear correlation coefficients of about −0.77 and −0.74 in the NH and SH, respectively, when the *Ap* time series is shifted by +1 day. It should be pointed out that the high correlation coefficients between *Ap*/OH and *Ap*/O_3 are primarily associated to the storm periods, which only represent about 25% of the data points. The main features of OH and O_3, presented in Figures 2a and 2b, are conserved if the filtering criterion for SPEs is lowered from 400 to 10 $cm^{-2}\,s^{-1}\,sr^{-1}$. The corresponding number of events is generally only slightly smaller by a few events (2–7), and changes of the maximum amplitudes at 75 km are negligible (<0.3%)

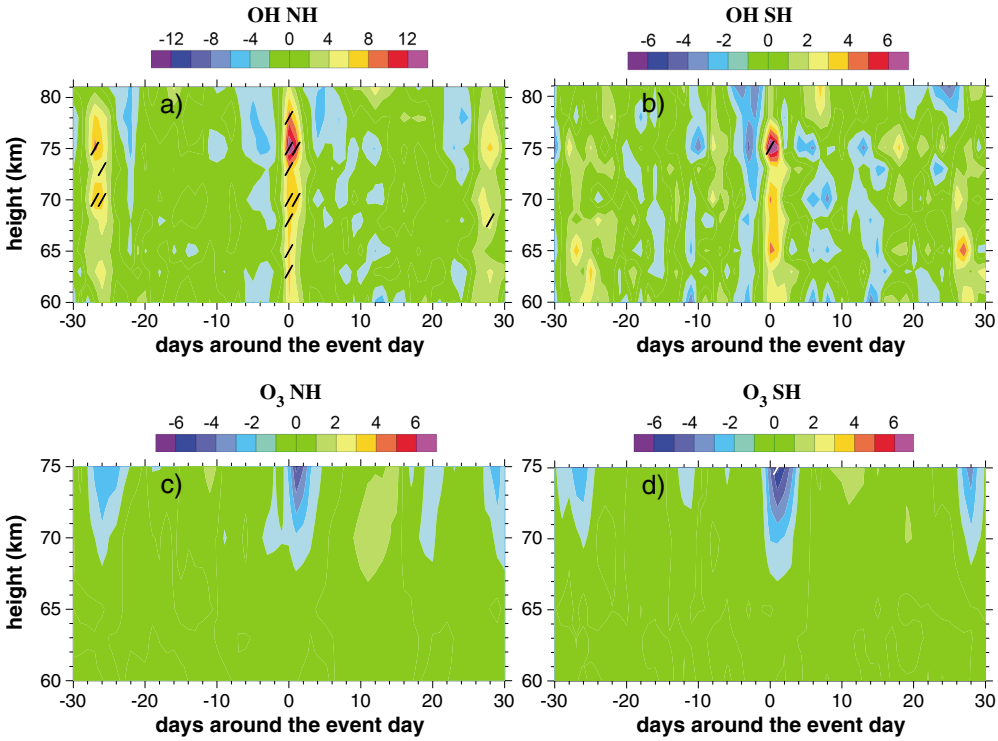

Figure 3. Nighttime trace gas amplitude (%) observed during winter conditions between 55° and 75° geomagnetic latitudes for OH/O_3 in (a and c) the Northern Hemisphere and (b and d) the Southern Hemisphere. The trace gas amplitudes were calculated by applying a superposed epoch analysis while using MLS Aura satellite nighttime measurements. Areas above 95% significance level are shaded in black (OH) and white (O_3). Note the different scaling of the *y* axis and the amplitude intervals.

except for the SH O_3 amplitude, which is damped by about 0.7%. However, this is not only caused by the additionally excluded SPEs but might also be attributed to the reduced number of events (200) compared to the original 228 events (see section 2.2).

While the OH chemical lifetime throughout the mesosphere is short (approximately seconds to minutes), the overall lifetime of HO_x can be up to hours due to the longer lifetime of H around 80 km and above. Our analysis of OH nighttime observations should not be affected by any daytime photochemical effects. Nevertheless, we conducted a sensitivity study to rule out possible influences from solar UV-induced OH signal. Therefore, Lyman alpha (Ly α) was used as a proxy for solar UV radiation and the SEA was repeated for daily Ly α observations. The corresponding results in both hemispheres for the sampling of the OH and O_3 observations (Figures 2e and 2f) reveal a 27 day signal, but the maxima are much broader and are also shifted by a few days compared to the respective *Ap* signatures. Occasionally, the increase or decrease of the Ly α signal does fit the respective response of the trace gas amplitudes; e.g., the Ly α rise in the NH around day -30 and day -3 approximately matches the increase/decrease of the OH/O_3 amplitude. However, in both cases the Ly α signal continues to grow and remains high even for a few days after the corresponding trace gas maxima. Furthermore, the Ly α signal drop is not visible in OH, while O_3 amplitudes become slightly positive. Thus, solar UV radiation influence cannot be completely ruled out for the entire period of ±30 days from these observations, but it is unlikely to influence the 27 day signatures in OH and O_3, whose timing and shape strongly resemble the *Ap* signal. Consequently, it is reasonable to conclude that the three maxima of the 27 day signal in OH and O_3 are primarily attributable to geomagnetic activity.

3.2. Altitude Dependency

In addition to the results presented in Figure 2, the SEA results of the entire height interval are displayed in Figures 3a–3d. The positive OH amplitude in the NH (Figure 3a) is present throughout the complete altitude interval and maximizes at 75 km, reaching +14% or about +0.1 ppb in absolute numbers if the respective OH

background is considered (see Figure 1a). The response generally lasts for 1–2 days, which could be probably attributed to occasionally longer-lasting high *Ap* events and the fact that the majority of energetic precipitating particles from CIR storms are usually delayed by a few days after the geomagnetic peak. These characteristics also hold for the secondary maxima at day ±27, which are about half as strong as the major one. The OH amplitudes at day 0 are generally above the significance level of 95% except for the lowermost and uppermost altitude level, while the secondary maxima only exceed this significance level from 70 to 75 km (day −27) and at 68 km (day +27). The three maxima of the OH amplitude exceed the precision error of <2% at nearly all heights, further supporting that the observed 27 day signal is an actual feature and not caused by measurement noise.

In the SH the OH amplitudes (Figure 3b) are generally smaller, on average reduced by a factor of 2 compared to those in the NH, and the overall response is noisier, possibly due to the smaller number of events (see section 2.1). Therefore, the 27 day cycle is less pronounced below 75 km and vanishes at altitudes above, but at least the clear OH amplitude maximum at 75 km at day 0 (~ +8%) is above the 95% significance level and additionally exceeds the precision error of ~1%. This interhemispheric asymmetry cannot be explained by differences in the geomagnetic activity, because Figure 2 shows that the corresponding SH winter *Ap* signal from 2004 to 2009 (21.0) is slightly stronger at day 0 compared to the respective peak in NH winter (18.9). Additionally, the 27 day cycle is also only a little less distinct in the SH than in the NH. These results of the OH amplitude in both hemispheres are, in general, in agreement with the observations reported by *Andersson et al*. [2012], who investigated the same OH data but used slightly different filter criteria. Note that they did not analyze the 27 day signal; however, their correlation analysis also showed best agreement between NH OH vmrs and electron precipitation at 70–78 km and substantially less pronounced structures in the SH. The interhemispheric difference could partly be attributed to the larger SH OH background during winter (see Figure 1a), because the presented OH amplitudes are relative deviations to the respective background. Consequently, even if the absolute variations between the two hemispheres during winter are small, the relative differences cannot be neglected. In detail, the SH winter OH background is larger by about ~75% at heights ≤70 km and about ~30% at altitudes above compared to the corresponding NH OH background. However, since the absolute OH variations are also higher in the NH (~0.07 ppb at day 0) than in the SH (~0.05 ppb at day 0), a different hemispheric forcing might play an additional role. It should be further considered that the MLS solar zenith angle sampling is not the same in both hemispheres, and an impact of the differences in time of day variations on night measurements cannot be ruled out. In fact, SH observations are performed during deeper night conditions at solar zenith angles between 114° and 128°, while the corresponding NH range is 108°–125°. Additionally, the higher SH OH background probably requires higher particle fluxes to cause measurable OH variations [*Verronen et al*., 2011]. This is discussed in more detail in section 3.3, but a final conclusion explaining the interhemispheric differences cannot be drawn at this point.

Figures 3c and 3d reveal that the negative O_3 impact due to geomagnetic activity in both hemispheres is restricted to altitudes >70 km. The maximum O_3 amplitudes are observed at 75 km and reach values of about −6 to −7% (−0.1 ppm absolute variation) at day +1 and approximately −2 to −3% for the secondary maxima at day −26 and +28. While only the SH major maximum at 75 km at day +1 is above the significance level of 95%, all three maxima in both hemispheres exceed the precision error of <0.5%. The influence of geomagnetic activity is already apparent at day 0 and is present until days 3 and 4, depending on altitude. In general, these observed features are in agreement with the results presented by *Andersson et al*. [2014], who, in contrast, reported a larger O_3 depletion because they only considered the largest 60 particle events in contrast to more than 200 events used in this study. The reason that no O_3 feedback is observed below 70 km is likely due to the generally low OH vmr (<0.5 ppb; see Figure 1a). The corresponding absolute OH variation induced by geomagnetic activity is therefore also small and probably cannot cause noticeable O_3 changes. Thus, the O_3 results are consistent with the presented OH observations and *Ap* measurements. The SEA was also carried out for ±90 days in order to investigate the behavior beyond the secondary peaks. The results further confirmed the solar rotational effect from geomagnetic activity on OH and O_3 (see Figure S1 in the supporting information).

The SEA was also performed for nighttime data during summer conditions (not shown here). The results reveal that the structure of the OH amplitude is more disturbed there. This could be attributed to the lower

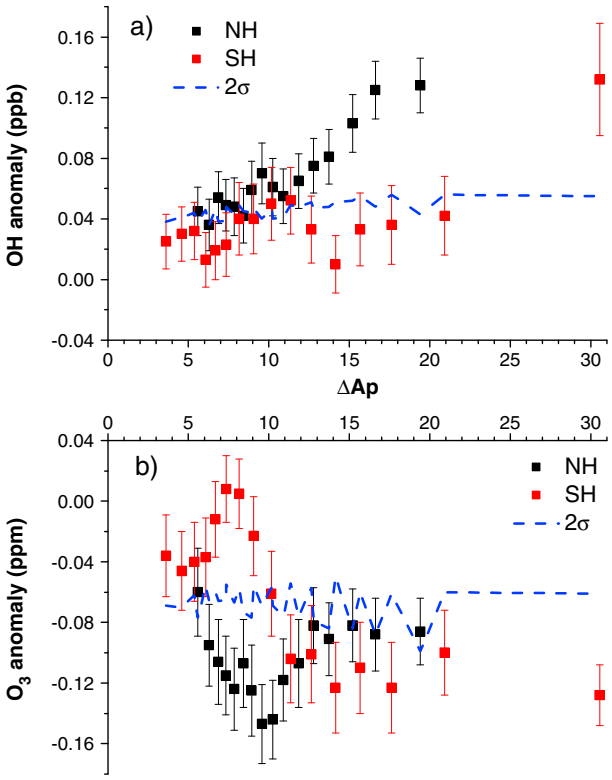

Figure 4. Superposed epoch analysis at 75 km for absolute OH/O_3 anomalies from (a/b) day 0/+1, as a function of the event magnitude (ΔAp). The 2σ confidence levels (dashed lines) and the errors of the mean of the corresponding trace gas amplitudes (error bars) are added.

data sampling due to shorter nights and does not originate from slightly different geomagnetic activity. Nevertheless, the NH major peak at day 0 exceeds the 2σ confidence level at altitudes >70 km, and the 27 day signal becomes especially apparent at 75 km, where all three maxima rise above 95% significance level. Again, SH OH response is essentially weaker and only significant at day 0 at 75 km. In contrast, the corresponding O_3 amplitude shows no response in either hemisphere, possibly resulting from the increased influence of solar radiation and the accompanying rapid O_3 recovery rates. Additionally, the SEA was also applied for OH and O_3 daytime measurements (solar zenith angle <88°), but a distinct 27 day solar rotational signal associated with geomagnetic activity was only observed for OH during winter above 70 km in the NH. The weaker/missing response of OH/O_3 in summer and during daytime is probably due to the increased influence of solar radiation. Since the major OH source in the mesosphere is the photolysis of water vapor, the relative impact of precipitating particles on OH is obviously stronger in winter and during night due to the lack of sunlight and thus lower OH background levels. O_3 exhibits rapid recovery rates when solar radiation is available. As reported by *Damiani et al*. [2006], measureable O_3 depletion occurs only for the first 12 h after an SPE. Obviously, such short-term O_3 reduction cannot be observed in the daily O_3 means used in this study.

3.3. Impact of *Ap* Increases on Trace Gas Amplitudes

In order to have a closer look into the relation between *Ap*, OH, and O_3 the focus was set on 2004–2009 to investigate the same events for both trace gases. In the next step all event days of both hemispheres were individually sorted from weak to strong events and grouped in 16 overlapping intervals of approximately equal number of 35 (NH) and 30 (SH), according to the ΔAp (difference between *Ap* value at the event day and the respective 27 day running *Ap* mean). Weakest events are primarily observed during the minimum of the 11 year solar cycle in 2009, while stronger ΔAp values are shifted to the years 2004–2005 when the Sun was more active. The SEA was repeated for each ΔAp group and carried out for winter conditions in the NH and SH. The corresponding results for OH (O_3) at day 0 (+1) at 75 km, as a function of the event magnitude (ΔAp), are shown in Figure 4. Here ΔAp is actually an arithmetic average of the respective interval. Note that absolute trace gas anomalies (difference between trace gas value at 1 day and the respective 27 day running mean) are displayed here to avoid differences due to the trace gas background and for direct comparisons between NH and SH. Furthermore, it is reasonable to assume that the particle precipitation impact on absolute vmrs of OH and O_3 primarily depends on the event magnitude and less on the geographic location.

The results reveal that the NH OH anomalies (Figure 4a) are nearly constant for $\Delta Ap < 11$ and mainly slightly above the 2σ confidence level (dashed line) but start to continuously increase for stronger events, showing a rise on average of about +0.12 ppb/10 ΔAp. This anomaly growth is significant, because the rise increases the error of the means of the respective OH vmrs (error bars). The pattern of the OH anomalies is generally similar in the SH, showing weak variations below 21 ΔAp but also a strong growth of ~0.09 ppb/10 ΔAp at larger values. Thus, OH anomalies are indicated to rise only after a certain threshold of geomagnetic activity is

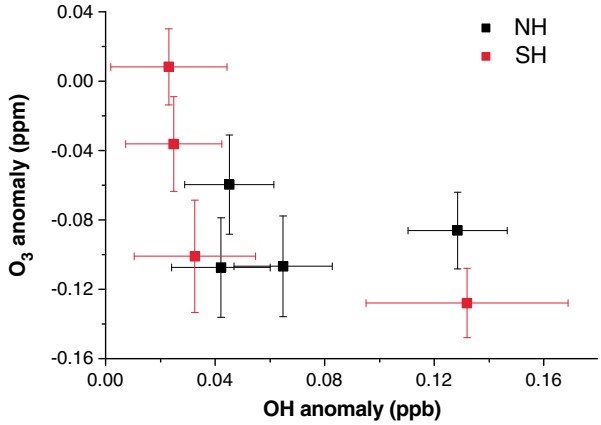

Figure 5. Scatterplot of the trace gas anomalies displayed in Figure 4 but only for every fourth anomaly to ensure the readability. The errors of the mean of OH and O_3 are added as horizontal and vertical error bars, respectively.

exceeded, while ΔAp and OH anomalies are not well correlated below this threshold. This behavior suggests that only geomagnetic disturbances above a certain magnitude lead to the generation of a sufficient amount of particles that can actually precipitate down to the mesosphere and produce measurable OH anomalies. The characteristic of an apparent threshold was also observed by *Verronen et al.* [2011] for electron count rates. They additionally found an increase of this threshold with increasing OH background since more particles are required to cause measurable OH anomalies in higher OH background concentrations. The shift of the threshold, depending on the OH background, is also seen here, because OH only responds to higher ΔAp in the SH in comparison to the NH, while the corresponding SH OH background increases NH OH background by about 30% (see Figure 1a). However, the SH OH growth is based on only two measurement points and is therefore not proven definitely, but these results are at least not in conflict with the observations reported by *Verronen et al.* [2011].

In contrast to OH, the O_3 results (Figure 4b) are noisier and the absolute anomalies already increase for weaker events. NH O_3 anomalies are usually above 95% significance level and show maximum values of about -0.15 ppm at 10 ΔAp after a strong negative rise of ~ -0.22 ppm/10 ΔAp. However, the O_3 response gets small for larger ΔAp, decreasing to -0.09 ppm. The SH O_3 anomalies reveal a significant negative growth of about -0.34 ppm/10 ΔAp, before reaching an elevated level ~ -0.11 ppm for $\Delta Ap > 11$. This observed saturated state, of which there is at least hint in the NH, is probably only valid for weak geomagnetic activity and accompanying small ionization rates, since SPE-related O_3 depletion can reach -70% [e.g., *Jackman et al.*, 2001] and SPEs represent stronger geomagnetic disturbances than considered in this study. Also, notable are the two positive anomalies close to 8 ΔAp, which are probably the result of the low number of event days (30–35). This leads to generally higher variability/noise, but reducing the number of analyzed intervals weakens the O_3 anomaly rise in the NH. A sensitivity test, using 11–16 partly overlapping intervals, confirmed that the general pattern presented in Figure 4 is robust (see Figure S2 in the supporting information).

Thus, the impact of precipitating particles on OH and O_3 is suggested to be nonlinear. In particular, no further O_3 depletion is observed for larger ΔAp, even though the corresponding OH anomalies increase. This nonlinear relation between OH and O_3 is investigated in more detail by plotting the trace gas anomalies shown in Figure 4 against each other (Figure 5). The pattern found implies that OH anomalies <0.04 ppb already lead to O_3 depletion, which might be due to a very efficient O_3 catalytic loss mechanism for small OH increases. After a certain O_3 reduction is reached (-0.1 to -0.15 ppm), a further increase of OH from 0.04 to 0.13 ppb has less effect on O_3. These characteristics were also observed at 70 km (not shown here), suggesting that the pattern is not a random feature. Consequently, the observed behavior might indicate that the reactions involving OH and O_3 have reached equilibrium, and additionally, produced OH does not further contribute to O_3 depletion. At this point, it should be considered that the HO_x catalytic reaction cycles, involving OH, H, and HO_2, destroy O_3 by reacting with O_3 and O (both known as active odd oxygen) and converting these odd oxygen species into less active O_2. When O_3 is rapidly depleted, overall odd oxygen concentration decreases, and the corresponding reaction rates for HO_x reaction cycles also decrease, making further O_3 depletion less effective. Therefore, an increase of OH will lead to stronger OH anomalies with respect to the corresponding O_3 anomalies, and consequently, the HO_x-O_3 system could easily reach equilibrium for weak OH enhancements. In addition, during these chemical processes, the partitioning of HO_x species could be altered, and consequently, OH alone would not be the best indicator for HO_x enhancements induced by geomagnetic activity. However, validating this hypothesis would require a detailed modeling beyond the scope of this

paper, and an altered partitioning of the HO_x species does not affect the observed results in regard to the individual relations between *Ap*/OH and *Ap*/O_3. It should be further considered that precipitating particle-induced HO_x production is accompanied by NO formation as well, which could in principal also contribute to the O_3 depletion, and an impact from NO enhancement on O_3 cannot be completely ruled out [*Sinnhuber et al*., 2012]. However, since NO_x species (=N + NO + NO_2) have a longer chemical lifetime compared to HO_x, their impacts are usually slower and extend to longer periods. Recent satellite measurements and model studies reported by *Jackman et al*. [2014] support the conclusion that the short-term O_3 depletion observed here is mainly caused by HO_x catalytic cycles rather than by long-lived NO_x species.

4. Conclusions

We have investigated nighttime OH (O_3) vmrs from 60 to 81 (60 to 75) km inside the geomagnetic latitudes connected to the outer radiation belts and the aurora region (55°N/S–75°N/S), using EOS Aura MLS satellite data from 2004 to 2009 (2004 to 2014). During NH winter we found a clear 27 day solar rotational cycle in OH measurements in-phase with geomagnetic activity (*Ap* signal), lasting for 1–2 days. Maximum amplitudes of +14% (~ +0.1 ppb) are observed at ~75 km, which exceed the significance level of 95%. The response is similar in the SH below 75 km, but it is essentially weaker (~ +8% at 75 km) and more disturbed, and additionally vanishes at higher altitudes. We could also show a distinct 27 day solar rotational signal observed in O_3 vmr in both hemispheres during winter, which is present for 3–5 days, depending on altitude. The O_3 signal lags in time by +1 day with respect to the *Ap* signal and is only apparent above 70 km but can be indeed attributed to geomagnetic activity-induced OH formation. The O_3 amplitudes also maximize at 75 km (−6 to −7%; ~ −0.1 ppm) but exceed the 95% significance level only in the SH. Since OH (O_3) amplitudes in both hemispheres exceed the precision error of 1–2% (<0.5%), the observed trace gas amplitudes are unlikely to originate from measurement noise. Absolute trace gas variations at 75 km in both hemispheres suggest that OH formation induced by precipitating particles is triggered by a certain magnitude of geomagnetic activity, which depends on the respective OH background. The corresponding OH impact on O_3 is indicated to be nonlinear and slows down for increasing OH anomalies. However, this might only be valid for the relatively weak geomagnetic activity and accompanying small ionization rates investigated here, since higher O_3 depletion of about −70% has been observed for large SPEs [e.g., *Jackman et al*., 2001]. Thus, we conclude that particle precipitation can cause measurable 27 day signal in nighttime mesospheric OH and O_3, if the influence of solar UV radiation is small and the magnitude of geomagnetic activity exceeds a certain threshold.

Acknowledgments

The data used in this study are completely freely accessible to the public and were downloaded from http://mls.jpl.nasa.gov/ (level 2 OH and O_3 measurements, version 3.3/3.4), http://www.ngdc.noaa.gov/geomag/data/poles/NP.xy (Earth's magnetic North Pole coordinates), http://umbra.nascom.nasa.gov/SEP/ (date of solar proton events), ftp://ftp.ngdc.noaa.gov/STP/GEOMAGNETIC_DATA/INDICES/KP_AP/ (daily *Ap* index values), and http://lasp.colorado.edu/lisird/lya/ (daily Lyman alpha values). Work at the Jet Propulsion Laboratory, California Institute of Technology, was done under contract with NASA. T. Fytterer and M. Sinnhuber gratefully acknowledge funding by the Helmholtz Association of German Research Centres (HGF), grant VH-NG-624. The authors further acknowledge support by Deutsche Forschungsgemeinschaft and Open Access Publishing Fund of Karlsruhe Institute of Technology.

Alan Rodger thanks the reviewers for their assistance in evaluating this paper.

References

Andersson, M. E., P. T. Verronen, S. Wang, C. J. Rodger, M. A. Clilverd, and B. R. Carson (2012), Precipitating radiation belt electrons and enhancements of mesospheric hydroxyl during 2004–2009, *J. Geophys. Res.*, *117*, D09304, doi:10.1029/2011JD017246.

Andersson, M. E., P. T. Verronen, C. J. Rodger, M. A. Cliverd, and A. Seppälä (2014), Missing driver in the Sun-Earth connection from energetic electron precipitation impacts mesospheric ozone, *Nat. Commun.*, *5*, 5197, doi:10.1038/ncomms6197.

Brasseur, G. P., and S. Solomon (2005), *Aeronomy of Middle Atmosphere*, 3rd ed., Springer, Dordrecht, Netherlands.

Chree, C. (1913), Some phenomena of sunspots and of terrestrial magnetism at Kew Observatory, *Philos. Trans. R. Soc. London, Ser. A*, *212*, 75–116.

Damiani, A., M. Storini, M. Laurenza, C. Rafanelli, E. Piervitali, and E. G. Cordaro (2006), Southern ozone variations induced by solar particle events during 15 January–5 February, *J. Atmos. Sol. Terr. Phys.*, *68*, 2042–2052, doi:10.1016/j.jastp.2006.03.010.

Damiani, A., M. Storini, M. Laurenza, and C. Rafanelli (2008), Solar particle effects on minor components of the Polar atmosphere, *Ann. Geophys.*, *26*, 361–370, doi:10.5194/angeo-26-361-2008.

Friederich, F., M. Sinnhuber, B. Funke, T. von Clarmann, and J. Orphal (2014), Local impact of solar variation on NO_2 in the lower mesosphere and upper stratosphere from 2007 to 2012, *Atmos. Chem. Phys.*, *14*, 4055–4064, doi:10.5194/acp-14-4055-2014.

Froidevaux, L., et al. (2008), Validation of Aura Microwave Limb Sounder stratospheric ozone measurements, *J. Geophys. Res.*, *113*, D15S20, doi:10.1029/2007JD008771.

Jackman, C. H., R. D. McPeters, G. J. Labow, and E. L. Fleming (2001), Northern Hemisphere atmospheric effects due to the July 2000 solar proton event, *Geophys. Res. Lett.*, *28*, 2883–2886, doi:10.1029/2001GL013221.

Jackman, C. H., C. E. Randall, V. L. Harvey, S. Wang, E. L. Fleming, M. López-Puertas, B. Funke, and P. F. Bernath (2014), Middle atmospheric changes caused by the January and March 2012 solar proton events, *Atmos. Chem. Phys.*, *14*, 1025–1038, doi:10.5194/acp-14-1025-2014.

Lary, D. J. (1997), Catalytic destruction of stratospheric ozone, *J. Geophys. Res.*, *102*, 21,515–21,526, doi:10.1029/97JD00912.

Livesey, N. J., et al. (2013), EOS MLS version 3.3 and 3.4 Level 2 data quality and description document, Technical Support, Jet Propul. Lab., California Inst. Technology, Pasadena, Calif.

Pickett, H. M., W. G. Read, K. K. Lee, and Y. L. Yung (2006), Observation of night OH in the mesosphere, *Geophys. Res. Lett.*, *33*, L19808, doi:10.1029/2006GL026910.

Pickett, H. M., et al. (2008), Validation of Aura Microwave Limb Sounder OH and HO_2 measurements, *J. Geophys. Res.*, *113*, D16S30, doi:10.1029/2007JD008775.

Richardson, I. G., E. W. Cliver, and H. V. Cane (2000), Sources of geomagnetic activity over the solar cycle: Relative importance of coronal mass ejections, high-speed streams, and slow solar wind, *J. Geophys. Res.*, *105*, 18,203–18,213, doi:10.1029/1999JA000400.

Ruzmaikin, A., M. L. Santee, M. J. Schwartz, L. Froidevaux, and H. M. Pickett (2007), The 27-day variations in stratospheric ozone and temperature: New MLS data, *Gephys. Res. Lett.*, *34*, L02819, doi:10.1029/2006GL028419.

Shapiro, A. V., E. Rozanov, A. I. Shapiro, S. Wang, T. Egorova, W. Schmutz, and T. Peter (2012), Signature of the 27-day solar rotation cycle in mesospheric OH and H_2O observed by Aura Microwave Limb Sounder, *Atmos. Chem. Phys.*, *12*, 3181–3188, doi:10.5194/acp-12-3181-2012.

Sinnhuber, M., H. Nieder, and N. Wieters (2012), Energetic particle precipitation and the chemistry of the mesosphere/lower thermosphere, *Surv. Geophys.*, *33*, 1281–1334, doi:10.1007/s10712-012-9201-3.

Solomon, S., D. W. Rusch, J. C. Gerard, G. C. Reid, and P. J. Crutzen (1981), The effect of particle precipitation events on the neutral and ion chemistry of the middle atmosphere: II. Odd hydrogen, *Planet. Space Sci.*, *29*, 885–892, doi:10.1016/0032-0633(81)90078-7.

Verronen, P. T., C. J. Rodger, M. A. Cliverd, and S. Wang (2011), First evidence of mesospheric hydroxyl response to electron precipitation from radiation belts, *J. Geophys. Res.*, *116*, D07307, doi:10.1029/2010JD014965.

Waters, J. W., et al. (2006), The Earth Observing System Microwave Limb Sounder (EOS MLS) on the Aura satellite, *IEEE Trans. Geosci. Remote Sens.*, *44*(5), 1075–1092, doi:10.1109/TGRS.2006.873771.